

Interplay of Biermann-battery and magnetic reconnection in 3-D colliding laser plasmas

J. Matteucci,^{1,*} W. Fox,^{1,2} A. Bhattacharjee,^{1,2} D. B. Schaeffer,¹
C. Moissard,³ K. Germaschewski,⁴ G. Fiksel,⁵ and S. X. Hu⁶

¹*Department of Astrophysical Sciences, Princeton University, Princeton, New Jersey 08540, USA*

²*Princeton Plasma Physics Laboratory, Princeton, NJ 08543, USA*

³*Laboratoire de Physique des Plasmas, École Polytechnique, Paris 75252, France*

⁴*Space Science Center, University of New Hampshire, Durham, New Hampshire 03824, USA*

⁵*Center for Ultrafast Optical Science, University of Michigan, Ann Arbor, Michigan 48109, USA*

⁶*Laboratory for Laser Energetics, University of Rochester, Rochester, New York 14623, USA*

(Dated: July 29, 2022)

Recent experiments have demonstrated magnetic reconnection between colliding plasma plumes, where the reconnecting magnetic fields were self-generated in the plasma by the Biermann battery effect. Using fully kinetic 3-D simulations, we show the full evolution of the magnetic fields and plasma in these experiments, including self-consistent magnetic field generation via the Biermann battery effect as well as advection and dilation of the field with the expanding plasmas. The collision of the two plasmas drives the formation of a current sheet, where reconnection occurs in a strongly time-and-space-dependent manner, demonstrating new 3-D reconnection mechanisms. At early times, we observe fast, vertically-localized Biermann-mediated reconnection, an inherently 3-D reconnection mechanism where localized heating in the reconnection layer coupled with the ablation density profile conspires to break field lines, reconnecting them downstream. At late times, fast reconnection is sustained by both the collisionless pressure tensor and the Biermann effect.

The Biermann Battery effect [1] is one of the few mechanisms known to spontaneously generate magnetic fields in plasmas. In the context of astrophysics, while too weak to generate the present-day observed cosmic magnetic fields by itself, the Biermann Battery effect is widely regarded as a possible source of the seed magnetic field, subsequently amplified by protogalactic turbulence [2]. In High Energy Density (HED) plasmas this effect has been shown to generate strong magnetic fields (10-100 T) during intense laser heating [3–11]. The extreme magnitude of the observed fields is a result of strong non-collinearity of density and temperature gradients ($\nabla n \times \nabla T$) which drive regions of net circulating electromotive force. In such experiments [3–5, 11], when two plumes are ablated adjacently, the oppositely polarized Biermann fields collide and undergo magnetic reconnection, the universal process in which magnetic fields threaded through plasma undergo a fundamental topological change, which results in often violent conversions of field energy into kinetic energy. HED laser plasmas provide a platform to broadly study magnetic reconnection, which is intrinsic to many phenomena throughout plasma physics [12], from the sawtooth instability in magnetic fusion confinement devices [13] to solar flares [14, 15] and disturbances in the Earth’s magnetosphere [16]. Indeed, recent HED experiments have observed many interesting effects associated with reconnection, including flux annihilation [4], stagnation of reconnection [11], and particle jets [3, 7]. However, the inherent 3-dimensionality of these experiments, on which the Biermann generation process entirely depends, has yet to be investigated. A natural question to ask regards the con-

tinued role of the Biermann battery effect during reconnection and energy conversion, given its importance for initially generating the fields. This line of investigation is also necessary in understanding the possible role of magnetic fields and reconnection in indirect and direct-drive inertial confinement fusion experiments, including the effect on energy partitioning and the modification of heat transport [17, 18].

In this Letter, we present the first end-to-end fully kinetic computational study of the 3-D magnetic reconnection in two recent HED experiments [3, 6], where field generation and evolution self-consistently follow from the ablation dynamics. Furthermore we demonstrate for the first time that the Biermann battery effect can play a direct role in 3-D magnetic reconnection, as we find the density and temperature profiles in the current sheet conspire to both destroy incoming flux and reconnect significant flux downstream via $\nabla n \times \nabla T$. We refer to this intrinsically 3-D process as “Biermann-mediated reconnection.” In the reconnection context, we note that the role of the electron pressure in the generalized Ohm’s law is long-known to be important in reconnection with a guide field, even in 2-D systems [19, 20]. However, the pressure physics presented here is intrinsically a 3-D effect, and therefore is ignored in standard 2-D reconnection models. We hypothesize that the findings may have important implications for reconnection and energy conversion in any 3-D reconnection systems, especially those with large density and temperature gradients such as in the presence of compressible plasma turbulence, as has been documented experimentally in the earth’s magnetosheath [21], the heliopause [22], and in simulations

of turbulent reconnection, including the highly turbulent reconnection upstream of high-mach number shocks [23]. In addition to these physics insights, we also demonstrate other 3-D effects in the system which are important for determining the rate of reconnection and energy conversion, including the role of vertical flux dilation to counteract flux pile-up in the reconnection layer [24].

Alongside HED experiments, fully kinetic simulations have proved to be an effective tool when investigating reconnection physics. Previous kinetic simulations of HED laser experiments based on model profiles have provided valuable insight into reconnection dynamics in this regime, including flux-pileup near the reconnection layer [24], plasmoid formation [25], the role of the Nernst effect in semi-collisional regimes [26], and particle acceleration by reconnection [27]. PIC simulations have also modeled Biermann magnetic field generation in expanding plasmas [28]. While one such study has investigated reconnection in electron-dominated (system size $L / d_{i0} \leq 1$) relativistic plasmas driven by short-pulse lasers [29], here we present the first end-to-end simulations in MHD regimes ($L / d_{i0} \gg 1$), capturing the time and spatially dependent field evolution characteristic of recent experiments driven by long-pulse lasers. For direct comparison, simulation results presented are modeled after two recent reconnection experiments at the Vulcan[3] and Shenguang-II (SG-II) laser facilities [3, 6], for each of which the relevant experimental parameters are presented in reference [30]. The generally good agreement between these simulations and experiments, including observed magnetic field strength and plasma evolution, supports the insights into the the reconnection process obtained by the simulations presented here.

We use a formulation of generalized Ohm's law in order to quantitatively account for the mechanisms involved in the generation, advection, and reconnection of the magnetic field. Via Faraday's law and generalized Ohm's law, the evolution of the magnetic field is described by

$$\frac{\partial \mathbf{B}}{\partial t} = \nabla \times \left[(\mathbf{v} \times \mathbf{B}) - \frac{\mathbf{j} \times \mathbf{B}}{n_e e} + \frac{\nabla p_e}{n_e e} + \frac{\nabla \cdot \mathbf{\Pi}_e}{n_e e} + \frac{\mathbf{R}_{ei}}{n_e e} \right], \quad (1)$$

where each term on the RHS has a physical interpretation. The ion flow and Hall terms solely advect the field and therefore preserve magnetic field lines. The third term, recognized as the Biermann battery term, which once the curl is taken can be written as $-\frac{1}{n_e e} \nabla n_e \times \nabla T_e$, generates (or destroys) field depending on the temperature, density, and field configurations. The traceless pressure tensor term ($\nabla \cdot \mathbf{\Pi}_e$), which is known to be very important in collisionless reconnection layers [31], includes the effect of viscosity as well as contributions from anisotropies between on-diagonal pressure components. \mathbf{R}_{ei} is the collisional momentum transfer between electrons and ions and includes both resistive diffusion and advection via the Nernst effect (via the thermal

force). As shown below, detailed analysis of the magnetic field evolution via Eq. 1 characterizes the role of the Biermann-battery effect to mediate reconnection alongside canonical pressure tensor mechanisms [31].

Simulation setup: We use the PSC code [32], a fully kinetic, explicit particle-in-cell code with Coulomb collisions, to model the two reference experiments. Simulations are initiated by heating a thin target with a model heating operator, obtaining expanding ablated plasma plumes. Correspondence of the simulation parameters with the physical system is obtained by matching the ion skin depth (evaluated at the ablation density) to the system size. The full simulation setup and scheme for modeling electron heating and plasma ablation is described in reference [30]. 3-D simulations include the outflow (Y) dimension in addition to the inflow (X) and vertical (Z) dimensions. For computational simplicity, each boundary is periodic where the inflow dimension is much shorter than the outflow and vertical dimensions. Similar to reference [30], we measure n_{ab} and T_{ab} to define the reference ion skin depth, $d_{i0} = (M_i/n_{ab} Z e^2 \mu_0)^{1/2}$ and the sound speed, $C_{s,ab} = (Z T_{ab}/M_i)^{1/2}$. Together these define the characteristic ablation timescale $t_d = d_{i0}/C_{s,ab}$, which, along with measured n_{ab} and T_{ab} , allows us to match PSC results to radiation-hydrodynamic simulations performed with the DRACO code [33]. This procedure converts our results to physical units, allowing us to connect directly with experimental observations.

We use a compressed electron-ion mass ratio, $Z m_e/M_i = 1/64$, and a compressed ratio between the electron thermal speed and speed of light $T_{ab}/m_e c^2 = 0.04$. We find that we are able to compress these values far below the physical ratios while achieving convergence in our results, so long as $Z m_e/M_i, T_{ab}/m_e c^2 \ll 1$. Ratios in 2-D down to $Z m_e/M_i = 1/400$ and in 3-D down to $Z m_e/M_i = 1/100$ have been checked for convergence with presented results in all cases excluding the 3-D SG-II simulation. In the Vulcan case, a grid of $25 \times 50 \times 150 d_{i0}$ is used, where the grid cell spacing is $< \frac{1}{3} d_{e0}, 2\lambda_{D,ab}$. At this scale, the target heating radius $R_H/d_{i0} = 2$, and bubble separation $L/d_{i0} = 25$. In the SG-II case, the grid dimensions are $80 \times 160 \times 480 d_{i0}$, with cell spacing of $< d_{e0}, 5\lambda_{D,ab}$, heating radius $R_H/d_{i0} = 12$, and bubble separation $L/d_{i0} = 80$. The collisionality, described by λ_{mfp} , the mean free path of electrons at T_{ab} and n_{ab} , is matched to the electron skin depth d_{e0} in order to preserve the correct collisional diffusivity of the magnetic field; $\lambda_{mfp}/d_{e0} = 12.5$ in the Vulcan simulation and $\lambda_{mfp}/d_{e0} = 20$ in the SG-II simulation. The comparison of these two setups shows how the evolution of reconnection depends on system size (L/d_i), where we expect more MHD-like behavior from the larger SG-II case.

Fig. 1 shows late time ($t = 25 t_d$) snapshots of the SG-II magnetized plume collision. Fig. 1 (a) shows a top-down view of the collision between the Biermann battery

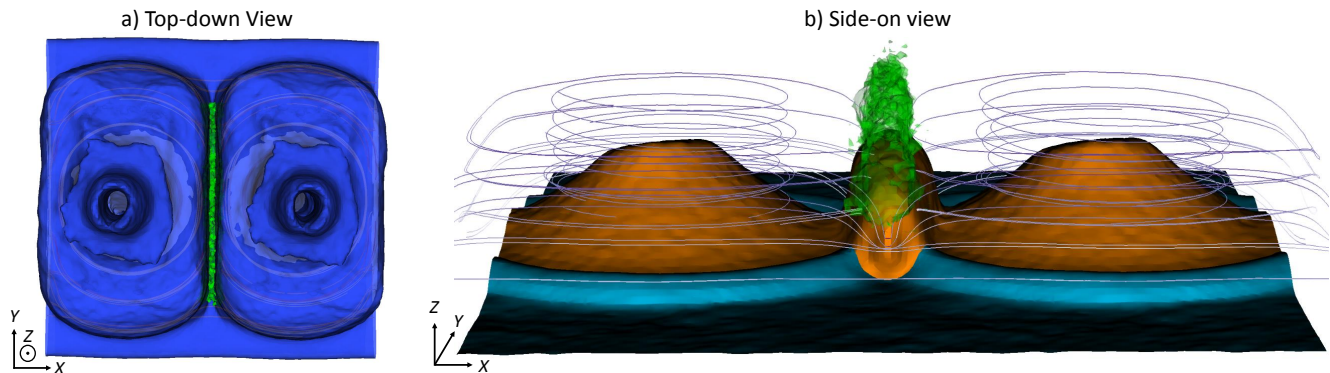


FIG. 1. Collision of two self magnetized plumes at the SG-II scale at time $25 t_d$. In (a) the blue contour represents $B^2/p_{ab} = 0.005$, green, $\mathbf{E} \cdot \mathbf{j}/(p_{ab}/t_d) = 0.001$. This panel displays the periodic nature of the simulation, where one plume has collided with itself, and two periods in X are shown. In b) the light blue contour represents $n_e/n_{ab} = 0.4$, orange, $p_e/p_{ab} = 0.07$, green is the same as in (a). Lines depict magnetic field lines, where field strength is indicated by color (purple to white.) Reconnected field lines in (b) show a strong vertical component, characteristic of Hall outflow.

generated fields represented by the blue surface. We observe magnetic fields generated up to 300 T in the SG-II case and 130 T at the Vulcan scale, comparable to the 370 T and 70-130 T estimated in each respective experiment [3, 7]. Fig. 1 (b) shows a contour of the electron pressure (orange) and density (light blue) from a side-on view, highlighting the 3-D behavior of the ablation and plume collision process of each plume. Magnetic reconnection is evidenced by the presence of downstream magnetic field energy as well as the non-zero $\mathbf{E} \cdot \mathbf{j}$ within the current sheet, representing a direct conversion of field energy into kinetic energy.

Fig. 2 shows the evolution of the reconnection current sheet at two different times. Fig. 2 (a) shows a 3-D visualization of T_e and n_e contours as the magnetic fields begin to collide. Fig. 2 (b-d), $t = 9 t_d$, and (f-h), $t = 25 t_d$, present the inflow plane profiles of n_e , T_e , and \mathbf{B}_{in} , where the heating is incident at the bottom edges of the view. We find that the Biermann battery generation continues to add upstream flux throughout the simulation; however, the generation mechanism is strongest during the initial heating. Fig. 2 (e, i) show \mathbf{B}_{out} along the outflow plane (at $x/d_{i0} = 0$), including a sharp structure of flux at $z \leq 20 d_{i0}$ and a more diffuse, extended structure from $z = 20 - 80 d_{i0}$. These two regions are clues to the multiple reconnection mechanisms operating in the simulation.

Biermann-mediated Reconnection: The profiles shown in Fig. 2 (a-d) demonstrate how Biermann-mediated reconnection takes place. At this time, the plumes are just beginning to interact; we observe the initial Biermann fields (strongest around $x = \pm 15 d_{i0}$) have been generated and are advecting toward the collision site. While the bulk plume densities have yet to collide, the reconnection process has already begun, as evidenced by the significant localized outflow field seen in Fig. 2 (a, d),

generated at $z = 5 - 10 d_{i0}$. At this time the reconnection layer has $\beta \approx 2$, where β is the ratio of plasma pressure to magnetic pressure. Seen in Fig. 2 (a, c) a localized hot spot has developed in the reconnection layer between the colliding magnetic fields, a result of hot electrons horizontally streaming in front of the fields. This hot spot flips the direction of ∇T_e in the current sheet to point toward the x-point rather than toward the plume. Given ∇n remains directed toward the high density target, the reversal of the temperature gradient leads $\nabla n \times \nabla T$ to change sign and destroy the incoming flux. The downstream temperature and density profiles likewise have outflow regions where ∇T_e points opposite the outflow, toward the collision site, leading $\nabla n \times \nabla T$ to create outgoing flux as ∇n remains toward the target. In Fig. 3 (a, b) the Biermann term ($-\frac{1}{n_e} \nabla n_e \times \nabla T_e$) is plotted in both the inflow and outflow plane. In addition to standard Biermann battery generation (seen at the edges from $x = \pm 10 - 40 d_{i0}$ in 3 a), we observe the localized reversal of the Biermann term, breaking field lines within the reconnection layer, close to the target. In Fig. 3 (b) we find the Biermann term generating significant downstream flux. Referring to Fig. 2 (d-e) we find the inflow and outflow fields correspond exactly to the Biermann destruction and creation terms.

Vertical Dilution: Fig. 2 (f-h) show the inflow profiles after the bulk densities have collided. The current sheet has now fully formed and thinned with the scale of the local d_i (local $d_i = 2 - 5 d_{i0}$, depending on vertical reconnection location.) At this time, inside the reconnection layer $\beta \approx 20$. Fig. 2 h) shows little pile-up in \mathbf{B}_{in} at the reconnection site; rather, the field is spread across the vertical. The reduction of flux pile-up is understood as a 3-D dilation effect caused by the ion advection term $\nabla \times (\mathbf{v} \times \mathbf{B})$, the $-B_y \partial V_z / \partial z$ component in particular, where flux dilates vertically and stacks, rather than

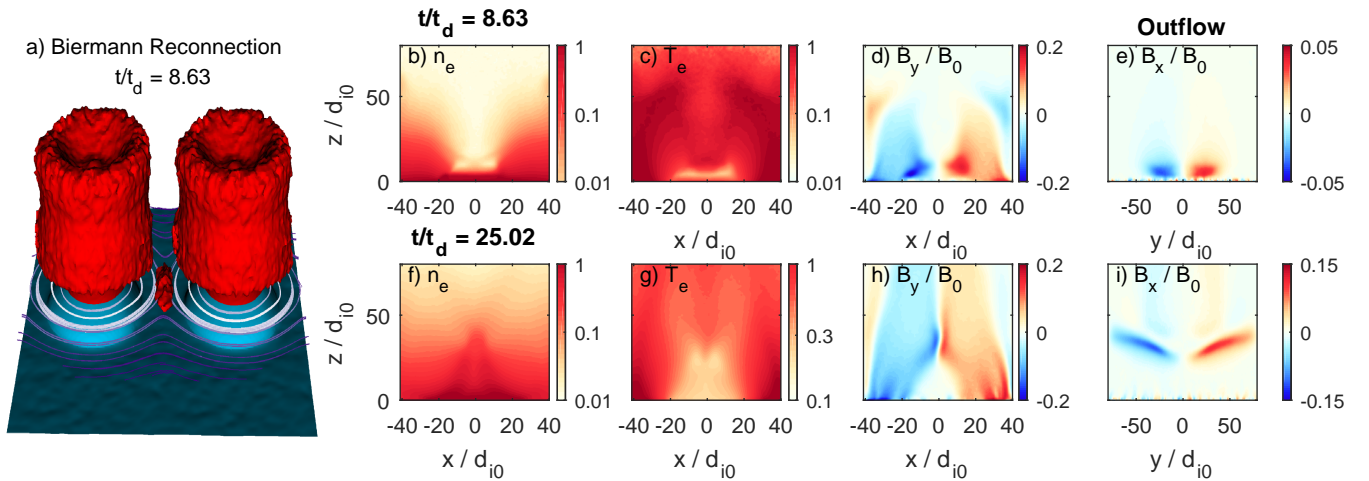


FIG. 2. a) 3-D visualization of the Biermann-mediated reconnection process, where two periods in X are shown. $T_e/T_{ab} = 0.5$ contour is shown in red, $n_e/n_{ab} = 0.4$ contour in light blue, and field lines are depicted. (b - d) 2-D slices along the inflow plane (x - z plane, $y = 0 d_{i0}$) of n_e and T_e , B_y for the collision of two 3-D magnetized plumes at the SG-II scale at time $t = 9 t_d$. Note: The view of the inflow profiles is cropped such that the left and right edges correspond to the centers of the left and right plumes, respectively. e) 2-D slice along the outflow plane (y - z plane, $x = 0 d_{i0}$) of the reconnected field B_x at the same time. (f-i) show similar plots to (b-e) at a later time, $t = 25 t_d$.

piling up horizontally. This results in “flux-stacking”, where the total vertically integrated flux increases, while the field strength locally does not pile-up significantly; a factor $1.5\times$ pile-up is observed in 3-D at both simulation scales vs. the $4\times$ pile-up observed in 2-D results.

We return now to analyze the second, more diffuse region of reconnected magnetic flux spanning from $z = 20 - 80 d_{i0}$ in Fig. 2 (i). Fig. 3 (c, d) shows that the inflow component of the collisionless pressure tensor term, $\frac{\partial^2 \Pi_{e_{xx}}}{n \partial x^2}$, related to electrons’ meandering orbits within the layer [34], is partially responsible for breaking field lines and reconnecting flux over this diffuse region. We note this is not the particular non-gyrotropic component that has been found responsible for fast collisionless reconnection in previous 2-D PSC reconnection simulations [24]. While it is tempting to directly connect this reconnection region with 2-D reconnection, a further inspection shows that the Biermann term intermittently plays a role in the reconnection in this region as well.

Fundamentally, the Biermann-mediated reconnection mechanism cannot operate in a simple 2-D reconnection scenario, as a density gradient along the reconnection x -line is required. Initially, we find Biermann-mediated reconnection to be localized near the target, with strong inflow driven by the Hall and Nernst effects, resulting in local reconnection rates of $0.1 B_{in} V_A$ (where the local $B_{in} V_A \approx 0.1 B_0 C_{s0}$); We find the vertically diffuse reconnection region, where reconnection is supported by both mechanisms, to have spatially and temporally dependent reconnection rates, ranging from $0.05 - 0.1 B_{in} V_A$ (where now, due to flux dilation, the local $B_{in} V_A \approx 0.03 B_0 C_{s0}$). The local rate slows as the current sheet thins but then

speeds up as two plasmoids develop and jet downstream at the local $V_A \approx 400$ km/s, in agreement with experimental observations of plasmoid jets [7]. Comparing the rate of overall flux reconnection in Fig. 3 (e), we find in both Vulcan and SG-II simulations that Biermann-mediated reconnection and collisionless pressure tensor reconnection contribute significantly.

The simulations shown in this Letter present novel insights into the 3-D physics of laser-driven reconnection experiments. In addition to MHD-scale HED experiments, we propose that Biermann-mediated reconnection is likely important in recent short-pulse experiments, where relativistic electrons are constrained to travel along the target surface [35]. In fact, reference [29] shows that the electron pressure tensor plays a large role, although the Biermann and off-diagonal pressure contributions were not separated in the Ohm’s law. Furthermore, Biermann-mediated reconnection and flux dilation could likely play a role in highly turbulent 3-D reconnection. This will be explored in future simulations at even larger system sizes characteristic of current experiments being performed at the OMEGA and NIF facilities, where 3-D plasmoid dynamics are predicted to play a role. Preliminary results indicate non-thermal particle energization is obtained during the Biermann-mediated reconnection, which will be reported in detail in future publications.

Simulations were conducted on the Titan supercomputer at the Oak Ridge Leadership Computing Facility at the Oak Ridge National Laboratory, supported by the Office of Science of the DOE under Contract No. DE-AC05-00OR22725. J. M. was supported by the ND-SEG Fellowship. This research was also supported by

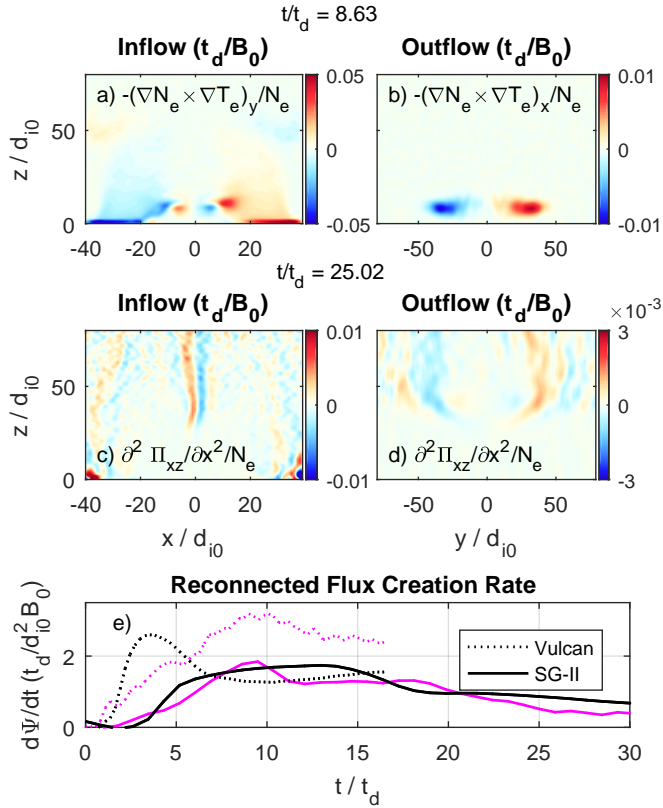


FIG. 3. a) 2-D slice along the inflow plane of the y -component of Biermann Battery term in Eq 1 at time $t = 9t_d$. b) the x -component of the Biermann term in the outflow plane at the same time. c) and d) show similar plots of the inflow non-gyrotropic electron pressure term in Eq 1 at a later time, $t = 24t_d$. e) shows the rate of flux creation ($\Psi = \int \frac{\partial B_{out}}{\partial t} dydz$) downstream of reconnection for the Biermann-mediated reconnection (black) and canonical quasi-2D collisionless reconnection (magenta) in both the Vulcan and SG-II simulations.

the DOE under Contracts No. DE-SC0006670, No. DE-SC0008655, and No. DE-SC0016249.

* jmatteuc@pppl.gov

[1] L. Biermann, *Z. Naturforsch* **5a**, 65 (1950).
 [2] R. M. Kulsrud, R. Cen, J. P. Ostriker, and D. Ryu, *Astrophys. J.* **480**, 481 (1997).
 [3] P. M. Nilson, L. Willingale, M. C. Kaluza, *et al.*, *Phys. Rev. Lett.* **97**, 255001 (2006).
 [4] C. K. Li, F. H. Séguin, J. A. Frenje, *et al.*, *Phys. Rev. Lett.* **99**, 055001 (2007).
 [5] L. Willingale, P. M. Nilson, M. C. Kaluza, *et al.*, *Phys. Plasmas* **17**, 043104 (2010).

[6] J. Zhong, Y. Li, X. Wang, *et al.*, *Nature Physics* **6**, 984 (2010).
 [7] Q. L. Dong, S. J. Wang, Q. M. Lu, *et al.*, *Phys. Rev. Lett.* **108**, 215001 (2012).
 [8] M. J.-E. Manuel, C. K. Li, F. H. Séguin, *et al.*, *Phys. Rev. Lett.* **108**, 255006 (2012).
 [9] L. Gao, P. M. Nilson, I. V. Igumenshev, *et al.*, *Phys. Rev. Lett.* **109**, 115001 (2012).
 [10] G. Fiksel, W. Fox, A. Bhattacharjee, *et al.*, *Phys. Rev. Lett.* **113**, 105003 (2014).
 [11] M. J. Rosenberg, C. K. Li, W. Fox, *et al.*, *Phys. Rev. Lett.* **114**, 205004 (2015).
 [12] M. Yamada, R. Kulsrud, and H. Ji, *Rev. Mod. Phys.* **82**, 603 (2010).
 [13] R. J. Hastie, *Astrophys. and Space Sci.* **256**, 177 (1997).
 [14] R. P. Lin and H. S. Hudson, *Solar Physics*, **50**, 153 (1976).
 [15] B. J. Anderson, T.-D. Phan, and S. A. Fuselier, *J. Geophys. Res.* **102**, 9531 (1997).
 [16] T. D. Phan, M. A. Shay, J. T. Gosling, *et al.*, *Geophys. Res. Lett.* **40**, 4475 (2013).
 [17] J. R. Rygg, F. H. Séguin, C. K. Li, *et al.*, *Science* **319**, 1223 (2008).
 [18] C. K. Li, F. H. Séguin, J. A. Frenje, *et al.*, *Science* **327**, 1231 (2010).
 [19] X. Wang, A. Bhattacharjee, and Z. W. Ma, *J. Geophys. Res.* **105**, 27633 (2000).
 [20] W. Fox, F. Sciortino, Stechow, J. Jara-Almonte, J. Yoo, H. Ji, and M. Yamada, *Phys. Rev. Lett.* **118**, 125002 (2017).
 [21] A. Retinò, D. Sundkvist, A. Vaivads, *et al.*, *Nature Physics* **3**, 236 (2007).
 [22] M. Opher, J. F. Drake, M. Swisdak, *et al.*, *Astrophys. J.* **734**, 71 (2011).
 [23] Y. Matsumoto, T. Amano, T. N. Kato, and M. Hoshino, *Science* **347**, 974 (2015).
 [24] W. Fox, A. Bhattacharjee, and K. Germaschewski, *Phys. Rev. Lett.* **106**, 215003 (2011).
 [25] W. Fox, A. Bhattacharjee, and K. Germaschewski, *Phys. Plasmas* **19**, 056309 (2012).
 [26] A. S. Joglekar, A. G. R. Thomas, W. Fox, and A. Bhattacharjee, *Phys. Rev. Lett.* **112**, 105004 (2014).
 [27] S. R. Titorica, T. Abel, and F. Fiuza, *Phys. Rev. Lett.* **116**, 095003 (2016).
 [28] K. M. Schoeffler, N. F. Loureiro, R. A. Fonseca, and L. O. Silva, *Phys. Rev. Lett.* **112**, 175001 (2014).
 [29] Y. L. Ping, J. Y. Zhong, Z. M. Sheng, *et al.*, *Phys. Rev. E* **89**, 031101 (2014).
 [30] W. Fox, J. Matteucci, C. Moissard, *et al.*, (2017), arXiv:1712.00152.
 [31] M. Hesse and D. Winske, *J. Geophys. Res.* **103**, 26479 (1998).
 [32] K. Germaschewski, W. Fox, S. Abbott, *et al.*, *J. Comp. Phys.* **318**, 305 (2016).
 [33] S. Hu, D. T. Michel, D. H. Edgell, *et al.*, *Phys. Plasmas* **20**, 032704 (2013).
 [34] T. W. Speiser, *J. Geophys. Res.* **70**, 4219 (1965).
 [35] A. Raymond, C. F. Dong, A. McKelvey, *et al.*, (2016), arXiv:1610.06866.